# Reservoir host immunology and life history shape virulence evolution in zoonotic viruses

**Authors:**
Cara E. Brook[1], Carly Rozins[2], Sarah Guth[3], Mike Boots[3,4]

**Affiliations:**
[1] Department of Ecology and Evolution, University of Chicago, Chicago, IL, USA
[2] Department of Science and Technology Studies, York University, Toronto, Canada
[3] Department of Integrative Biology, University of California, Berkeley, Berkeley, CA, USA
[4] Biosciences, University of Exeter, Penryn Campus, UK. TR10 9FE

**Corresponding author:** Cara E. Brook
**Email**: cbrook@uchicago.edu

**Author contributions:**
CEB and MB conceptualized the research. CEB carried out the modeling and analysis with contributions from CR and SG. CEB and CR wrote the materials and methods and Supplementary Appendix. CEB wrote the first draft of the main manuscript, which all authors edited and revised.

**Competing interest statement:** The authors have no competing interests to declare.

**Classification:** Biological sciences: Population biology.

**Key Words**
bat virus, spillover, virulence evolution, tradeoff theory

**Abstract**

The management of future pandemic risk requires a better understanding of the mechanisms that determine the virulence of emerging zoonotic viruses. Meta-analyses suggest that the virulence of emerging zoonoses is correlated with but not completely predictable from reservoir host phylogeny, indicating that specific characteristics of reservoir host immunology and life history may drive the evolution of viral traits responsible for cross-species virulence. In particular, bats host viruses that cause higher case fatality rates upon spillover to humans than those derived from any other mammal, a phenomenon that cannot be explained by phylogenetic distance alone. In order to disentangle the fundamental drivers of these patterns, we develop a nested modeling framework that pinpoints mechanisms which underpin the evolution of viral traits in reservoir hosts that cause virulence following cross-species emergence. We apply this framework to generate virulence predictions for viral zoonoses derived from diverse mammalian reservoirs, successfully recapturing corresponding virus-induced human mortality rates reported in the literature. Notably, our work offers a mechanistic explanation for the extreme virulence of bat-borne zoonoses and, more generally, demonstrates how key differences in reservoir host longevity, viral tolerance, and constitutive immunity impact the evolution of viral traits that cause virulence following spillover to humans. Our theoretical framework offers a series of testable questions and hypotheses designed to stimulate future work comparing cross-species virulence evolution in zoonotic viruses derived from diverse mammalian hosts.

**Significance Statement**

Bats are the natural reservoir hosts for zoonotic viruses that cause higher case fatality rates in humans than do viruses derived from any other mammal or bird host. Using a nested population-level and within-host modelling approach, we generate virulence predictions for viral zoonoses derived from diverse mammalian reservoirs, successfully reproducing human case fatality rates from zoonoses reported in the literature. Our model provides a mechanistic explanation for the virulence of bat-borne zoonoses and a general predictive framework to forecast the virulence of cross-species viral infections from diverse mammalian hosts.

## Main Text

### Introduction

The devastating impact of the SARS-CoV-2 pandemic highlights the extreme public health outcomes that can result upon cross-species emergence of zoonotic viruses. Estimating the relative threats posed by potential future zoonoses is an important but challenging public health undertaking. In particular, efforts to predict the virulence of emerging viruses can be complicated since chance will always play a role in dictating the initial spillover that precedes selection (1), virulence upon emergence may be maladaptive in novel hosts (2, 3), and patterns in available data may be muddled by attainment bias if avirulent infections go underreported (1). Nonetheless, a growing body of recent work highlights clear associations between reservoir and spillover host phylogeny and the virulence of a corresponding cross-species infection (4–7). In many cases, increasing phylogenetic distance between reservoir and spillover hosts is correlated with higher virulence infections (4–6), suggesting that spillover host immune systems may be poorly equipped to tolerate viral traits optimized in more distantly-related reservoirs. Still, the effect of phylogeny on spillover virulence appears to supersede that of phylogenetic distance alone (7, 8), indicating that taxon-specific reservoir host immunological and life history traits may be important drivers of cross-species virus virulence. Notably, bats host viruses that cause higher human case fatality rates than zoonoses derived from other mammals and birds, a phenomenon that cannot be explained by phylogenetic distance alone (8). Understanding the mechanisms that select for the evolution of unique viral traits in bats compared to those selected in other mammalian reservoirs should enable us to better predict the virulence of future zoonotic threats.

Although the disproportionate frequency with which the Chiropteran order may source viral zoonoses remains debated (9, 10), the extraordinary human pathology induced by many bat-borne zoonoses—including Ebola and Marburg filoviruses, Hendra and Nipah henipaviruses, and SARS, MERS, and SARS-CoV-2 coronaviruses (11)—is not contested. Remarkably, bats demonstrate limited clinical pathology from infection with viruses that cause extreme morbidity and mortality in other hosts (12). Bats avoid pathological outcomes from viral infection via a combination of unique resistance and tolerance mechanisms, which, respectively, limit the viral load accrued during infection ('resistance') and reduce the disease consequences of a given viral load ('tolerance') (13–16). Viral resistance mechanisms vary considerably across bat species; those described to date include: receptor incompatibilities that limit the extent of infection for certain viruses in certain bats (17–20), constitutive expression of antiviral cytokines in some bat species (21), and enhanced autophagy (22) and heat-shock protein expression (23) in others. While these extensive inflammatory responses would be pathological in most mammals, bats—as the only mammals capable of powered flight—have evolved numerous unique mechanisms of mitigating inflammation incurred during the intensive physiological process of flying (24–26). These anti-inflammatory adaptations include loss of PYHIN (27–29) and downregulation of NLRP3 (30) inflammasome-forming gene families, dampened STING-dependent interferon activation (31), and diminished caspase-1 inflammatory signaling (32). In addition to facilitating flight, this resilience to inflammation has yielded the apparent by-products of extraordinarily long bat lifespans (33) and tolerance of the immunopathology that typically results from viral infection (11). Moreover, recent work demonstrates how high virus growth rates easily tolerated in constitutively antiviral bat cells cause significant pathology in cells lacking these constitutive antiviral defenses (34). The extent to which inflammatory tolerance may modulate the evolution of the viruses that bats host, however, remains largely unexplored.

Modern theory on the evolution of virulence typically assumes, either explicitly or implicitly, that high pathogen growth rates should both enhance between-host transmission and elevate infection-induced morbidity or mortality, resulting in a trade-off between virulence and transmission (35–37). Theory further suggests that because viral 'tolerance' mitigates virulence without reducing viral load, most host strategies of tolerance should select for higher growth rate pathogens that achieve gains in between-host transmission without causing damage to the original host (37–39) (Fig. 1). The widely touted viral tolerance of bats (11, 16, 40–42) should therefore be expected to support the evolution of enhanced viral growth rates, which—though avirulent to bats—may cause significant pathology upon spillover to hosts lacking unique features of bat immunology and physiology. Beyond tolerance, other life history characteristics unique to diverse reservoir hosts likely also impact the evolution of traits in the viruses they

host—with important consequences for cross-species virulence following spillover. To date, we lack a specific theory that examines the relative impact of reservoir host life history on spillover virulence. Here, we explore the extent to which the immunological and life-history traits of mammalian reservoirs can explain variation in the virulence of zoonotic viruses emerging into human hosts.

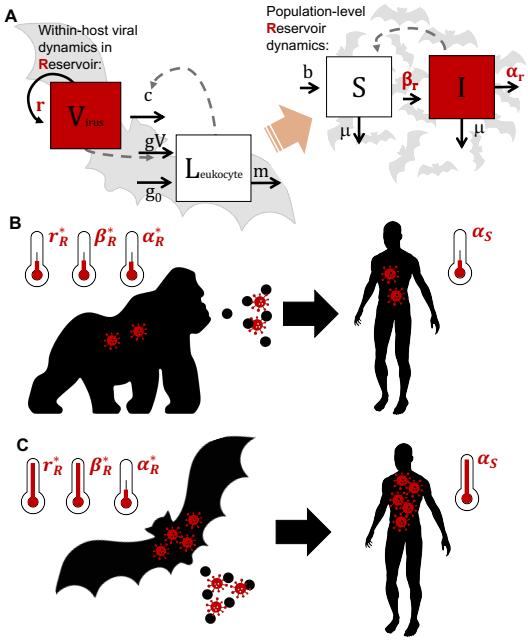


**Figure 1. Conceptual mechanistic framework to predict zoonotic virus virulence from reservoir immunology and life history traits.** (**A**) A within-host predator-prey model of leukocyte-virus dynamics is embedded in a population-level transmission model for reservoir hosts. Between-host rates of transmission ($\beta_r$) and virulence ($\alpha_r$) are expressed as functions of within-host dynamics to derive optimal virus growth rates in the reservoir ($r_R^*$). (**B**) Virus growth rates ($r_R^*$) evolve to maximize gains in between-host transmission ($\beta_R^*$) over virulence incurred on the reservoir ($\alpha_R^*$). Viruses evolved in taxa with physiologies similar to humans (i.e. non-human primates) should optimize at relatively low growth rates ($r_R^*$) that yield minimal pathology for the reservoir host ($\alpha_R^*$) and are, correspondingly, likely to cause only minimal pathology in the spillover human host ($\alpha_S$). (**C**) As a result of unique bat virus tolerance, viruses evolved in bat reservoir hosts may optimize at high $r_R^*$ values that maximize bat-to-bat transmission ($\beta_R^*$) but cause only minimal pathology in the bat host ($\alpha_R^*$) – but are likely to generate extreme virulence upon spillover ($\alpha_S$) to secondary hosts, including humans, that lack bat life history traits.

## Results

### *General trends in the evolution of high growth rate viruses.*

To elucidate how immunological and life-history traits of mammalian hosts combine to drive zoonotic virus virulence, we adopted a nested modeling approach, embedding a simple within-host model of viral and leukocyte dynamics within an epidemiological, population-level framework (Fig. 1). We examined how the life history traits of a primary reservoir drive the evolution of viral traits likely to cause pathology in a secondary, spillover host—chiefly, a human. Using our nested model in an adaptive dynamics framework (43), we first expressed the conditions—called the 'invasion fitness'—which permit invasion of an evolutionarily 'fitter', mutant virus into a reservoir host system in within-host terms. This allowed us to calculate the optimal within-host virus growth rate ($r^*$) for a virus evolved in reservoir hosts that differ across a suite of life history traits and corresponding cellular and immunological parameters (Fig. 2; Table 1; *SI Appendix* Fig S1-S2). In part with this optimization, we also calculated the corresponding transmission ($\beta^*$) and virulence ($\alpha^*$) for the reservoir host at the optimal $r^*$(Fig. 2; Table 1; *SI Appendix* Fig S1-S2). We derive the equation for the optimal virus growth as follows:

$$r^* = \frac{cg_0}{m} + \frac{\sqrt{c^2m^2gg_0\mu T_vT_w(vT_w+gwT_v)}}{m^2(vT_w+gwT_v)},$$

where $\mu$ signifies the natural mortality rate of the reservoir host, and all other parameters represent within-host viral and immune dynamics in a persistently infected reservoir. Thus, $c$ corresponds to the rate of virus clearance by leukocytes, $g_0$ is the magnitude of constitutive immunity, $m$ is the natural leukocyte mortality rate, and $g$ is the rate of leukocyte activation following infection. The parameters $v$ and $w$ correspond, respectively, to the intrinsic virulence of the virus and the reservoir host's natural susceptibility to inflammatory damage, while $T_v$ and $T_w$ represent reservoir host tolerance to direct virus pathology and to immunopathology. We present all main text results under assumptions by which tolerance manifests as a *constant* reduction of either direct virus-induced pathology ($T_v$) or immunopathology ($T_w$). See *SI Appendix* for comparable results under assumptions of *complete* tolerance, whereby tolerance completely eliminates virus pathology and immunopathology up to a threshold value, beyond which pathology scales proportionally with virus and immune cell growth.

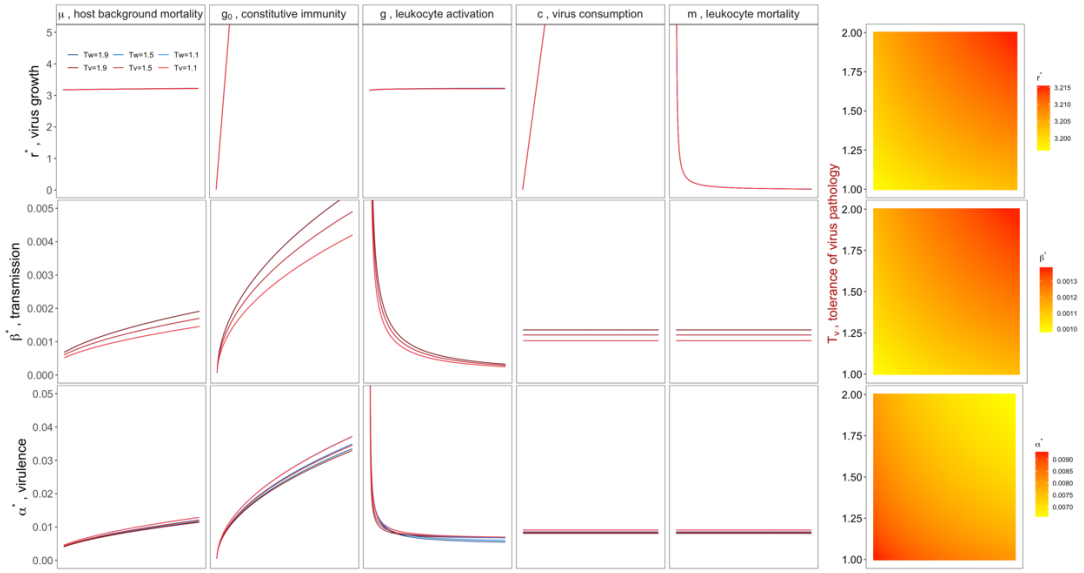


**Figure 2. Optimal virus growth rates vary across reservoir host immunological and life history parameters.** Rows (top-down) indicate the evolutionarily optimal within-host virus growth rate ($r^*$) and the corresponding between-host transmission rate ($\beta^*$), and virus-induced mortality rate ($\alpha^*$) for a reservoir host infected with a virus at $r^*$. Columns demonstrate the dependency of these outcomes on variable reservoir host parameters: background mortality ($\mu$), magnitude of constitutive immunity ($g_0$), rate of leukocyte activation upon viral contact ($g$), rate of virus consumption by leukocytes ($c$), and leukocyte mortality rate ($m$). Darker colored lines depict outcomes at higher tolerance of direct virus pathology ($T_v$, red) or immunopathology ($T_w$, blue), assuming no tolerance of the opposing type. Heat maps demonstrate how $T_v$ and $T_w$ interact to produce each outcome. Parameter values are reported in Table 1. Figure assumes tolerance in the 'constant' form (see *SI Appendix,* Fig. S2 for 'complete' tolerance assumptions).

Our analyses highlight several critical drivers of virus evolution likely to generate significant pathology following spillover to a secondary host (Fig. 2): higher within-host virus growth rates ($r^*$) are selected in reservoir hosts with higher background mortality ($\mu$), elevated constitutive immune responses ($g_0$), more rapid leukocyte activation upon infection ($g$), and more rapid virus clearance by the host immune system ($c$). Additionally, higher $r^*$ viruses are selected in hosts exhibiting lower leukocyte mortality rates ($m$), resulting in longer-lived immune cells. Critically, higher tolerance of both virus-induced pathology ($T_v$) and immunopathology ($T_w$) also select for higher $r^*$ when virulence due to direct virus damage and to immunopathology are modeled, respectively, as proportional to virus and immune cell growth rates (*SI Appendix*). In keeping with trade-off theory, changes in the majority of within-host parameters drive corresponding increases in $r^*$, $\beta^*$, and $\alpha^*$, such that viruses evolved to high growth rates experience high transmission within the reservoir host population—but also generate high virus-induced mortality (Fig. 1). By definition, the two modeled mechanisms of tolerance ($T_v$ and $T_w$) decouple the relationship between transmission and virulence, permitting evolution of high $r^*$ viruses that achieve gains in between-host transmission in the reservoir population ($\beta^*$), while simultaneously incurring minimal virulence ($\alpha^*$) on reservoir hosts. By extension, we predict that viruses evolving high optimal $r^*$ values in reservoir hosts

with high $T_v$ or $T_w$ might incur substantial pathology upon spillover to secondary hosts exhibiting reduced tolerance as compared with the reservoir.

***Order-specific estimates for optimal virus growth rates evolved in reservoir hosts.***
We next applied our model to make broad predictions of the evolution of optimal virus growth rates across diverse mammalian reservoir orders, based on order-specific variation in three key parameters from our nested model: the reservoir host background mortality rate ($\mu$), the reservoir host tolerance of immunopathology ($T_w$), and the magnitude of constitutive immunity ($g_0$). Within-host immunological data needed to quantify these parameters is lacking across most mammalian orders; thus, we applied generalized additive models (GAMs (44)) to mammalian life history data—in particular, well-described allometric relationships between mammalian body mass and basal metabolic rate (BMR) with lifespan and immune cell concentrations (45–49)—to proxy $\mu$, $T_w$, and $g_0$ across diverse mammalian orders (Fig. 3A-C; Table 1; *SI Appendix,* Fig. S3-S4).

Fitted GAMs demonstrated a statistically significant positive association between the orders Chiroptera, Cingulata, Monotremata, and Primates and the response variable of maximum longevity, indicating that species in these orders exhibit, on average, longer lifespans than predicted for their body sizes (Fig. 3A; *SI Appendix,* Fig. S3; Table S1-S2). By contrast, six mammalian orders (Afrosoricida, Dasyuromorphia, Didelphimorphia, Eulipotyphla, Notoryctemorphia, and Peramelemorphia) showed significantly shorter lifespans than predicted for body size (Fig. 3A; *SI Appendix,* Fig. S3; Table S1-S2). Fitted GAMs further demonstrated a statistically significant positive association between the orders Chiroptera and Monotremata and the response variable of baseline neutrophil concentration, indicating that species in these orders may have more enhanced constitutive immune responses than predicted by mass-specific BMR. The orders Cetartiodactyla, Dasyuromorphia, Diprotodontia, and Scandentia, by contrast, showed significant negative associations, representing lower baseline neutrophil concentrations than predicted per mass-specific BMR (Fig. 3B; *SI Appendix,* Fig. S3; Table S1-S2).

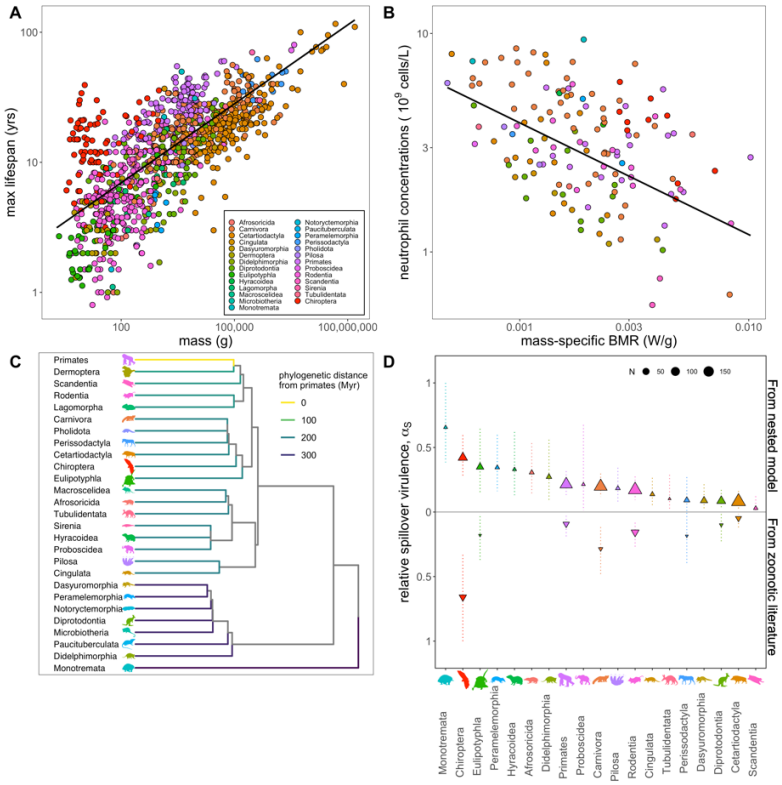


**Figure 3. Reservoir host life history traits predict evolution of zoonotic virus virulence.** (**A**) Variation in $\log_{10}$ maximum lifespan (y-axis, in years) with $\log_{10}$ adult body mass (x-axis, in g) across mammals, with data derived from Jones et al. 2009 (56) and Healy et al. 2014 (57). Points are colored by mammalian order, corresponding to legend. Black line depicts predictions of mammalian lifespan per body mass, summarized from fitted GAM (but excluding random effect of mammalian order), presented in

*SI Appendix*, Table S2. Order-level parameters for nested modeling parameters of average annual mortality rate ($\mu$) and tolerance of immunopathology ($T_w$) were derived, respectively, by taking the inverse of the predicted lifespan per order from the fitted GAM ($\mu$) and calculating the scaled effect of order on maximum lifespan ($T_w$) (*SI Appendix*, Fig. S3-S4; Table S1-S2). (**B**) Baseline neutrophil concentrations (y-axis, in $10^9$ cells/L) per mass-specific metabolic rate (x-axis, in W/g) across mammals, with data from Jones et al. 2009 (56) and Healy et al. 2014 (57) combined with neutrophil concentrations from Species360 (49). Black line projects neutrophil concentration per mass-specific metabolic rate (excluding random effects of mammalian order), simplified from fitted GAM presented in *SI Appendix*, Table S2. An order-level estimate for the nested modeling parameter of the magnitude of constitutive immunity ($g_0$) was derived from the scaled effect of order on $\log_{10}$ neutrophil concentration per $\log_{10}$ body mass (in g), combined with BMR (in W) (*SI Appendix*, Fig. S3-S4; Table S1-S2). (**C**) Phylogenetic distance from Primates ($\eta_R$, in millions of years, indicated by color) on a timescaled phylogeny, using data from TimeTree (83). An order-level estimate for the nested modeling parameter of the spillover human host tolerance of pathology induced by a virus evolved in a different reservoir order ($T_{vS}$) was estimated as the scaled inverse of this phylogenetic distance (*SI Appendix*, Fig. S4; Table S1). (**D**) Comparison of relative human spillover virulence ($\alpha_S$) predictions for zoonoses from nested life history model with estimates from the literature. Top panel depicts relative human $\alpha_S$ predictions by order, derived from within-host model, using order-specific parameters for $\mu$, $T_w$, $g_0$, and $T_{vS}$ (*SI Appendix*, Table S1). Bottom panel depicts relative human $\alpha_S$ estimates derived from case fatality rates and infection duration reported in the zoonotic literature (8). For the top panel, point size corresponds to the average number of species-level datapoints (N) used to generate each of the four variable parameters impacting $\alpha_S$. For the bottom panel, point size indicates the total number of independent host-virus associations from which virulence estimates were determined. 95% confidence intervals were computed by standard error; for top panel, these reflect the upper and lower confidence intervals of the optimal virus growth rate. See *SI Appendix,* Table S1 for order-level values for $r^*$, $\mu$, $T_w$, $g_0$, and $T_{vS}$ and Table 1 for all other default parameters involved in calculation of $\alpha_S$.

We generated an estimate of background mortality ($\mu$) for 26 disparate mammalian orders by taking the inverse of predicted lifespan (in days) per order from our first fitted GAM, excluding the effects of body size (*SI Appendix,* Fig. S4; Table S1). Since longevity and resilience to inflammation are linked extensively in the literature (11, 42, 50–53), we represented our $T_w$ parameter as the scaled effect of these 26 mammalian orders on the predicted lifespan per body size—such that orders longer-lived than predicted were modeled with high values for tolerance to immunopathology and vice versa. As a result, order-level estimates for $\mu$ and $T_w$ were mirror inverses of one another: bats, for instance, demonstrated the lowest predicted values across all orders for background mortality ($\mu$) and the highest predicted values for tolerance of immunopathology ($T_w$) (*SI Appendix,* Fig. S4; Table S1). Because our nested model expressed parameters in timesteps most relevant to viral dynamics (days), differences in mortality rates across mammalian orders—though substantial on multi-year timescales of the host—had limited influence on downstream predictions of differences in the evolution of virus growth rates. This result echoed prior observations from Fig. 2, which showed reduced sensitivity of $r^*$ to realistic variation in the magnitude of $\mu$, as compared with other parameters.

Building from our approach for $T_w$, we next generated order-level estimates for the parameter $g_0$, which represents the magnitude of constitutive immune response of the reservoir host in our nested modeling framework. We calculated $g_0$ as the scaled effect of mammalian order on the prediction of neutrophil concentration per mass-specific metabolic rate from our second fitted GAM for the 19 orders for which we possessed paired neutrophil and BMR data (*SI Appendix,* Fig. S4; Table S1). Orders Chiroptera and Monotremata, which showed significantly higher neutrophil concentrations than predicted by mass-specific BMR, were thus modeled with high $g_0$, while orders Cetartiodactyla, Dasyuromorphia, Diprotodontia, and Scandentia, which exhibited lower neutrophil concentrations than predicted, were modeled with low $g_0$ (*SI Appendix,* Fig. S4; Table S1).

Finally, we combined order-specific parameters for $\mu$, $T_w$, and $g_0$ with fixed parameter values for all other within-host terms to generate an estimate of the optimal growth rate of a virus evolved in the 19 mammalian orders for which we possessed proxy data for all three variable within-host parameters (Table 1; *SI Appendix,* Fig. S5; Table S1). We termed this reservoir-host optimized virus growth rate, $r_R^*$ (Fig. 1B-C). In keeping with predictions from our general model (Fig. 2), we predicted the evolution of high $r_R^*$ viruses from reservoir orders exhibiting high $\mu$, $T_w$, and/or $g_0$. Since $\mu$ and $T_w$ were inversely correlated but within-host dynamics more sensitive to changes in $T_w$, we ultimately recovered the highest predicted optimal growth rates for viruses evolved in the orders Chiroptera and Monotremata, which exhibited both long lifespans per body size and high baseline neutrophil concentrations. Data were particularly sparse, however, for order Monotremata, for which complete records were only available for two species (the platypus and the short-beaked echidna). As a result, predictions for this order should be interpreted with caution. More data, particularly for baseline neutrophil concentrations, will be needed to evaluate the

extent to which these predictions hold across all five extant species in the Monotremata order. Additionally, we predicted the evolution of the lowest growth rate viruses in reservoir hosts of the orders Cetartiodactyla, Dasyuromorphia, Diprotodontia, and Scandentia, largely as a result of significantly low values estimated for the magnitudes of constitutive immunity in these orders.

***Estimating zoonotic virus virulence in spillover human hosts.***
After establishing optimal growth rates for viruses evolved in diverse reservoir host orders ($r_R^*$), we subsequently modeled the corresponding 'spillover virulence' ($\alpha_S$) of these viruses following emergence into a human host. Zoonotic spillovers were modeled as acute infections in the human, and virulence was calculated while varying only the growth rate of the spillover virus ($r_R^*$) and the human tolerance of direct virus pathology ($T_{vS}$) between viruses evolved in differing reservoir orders. We varied this last parameter, $T_{vS}$, to account for any differences in virus adaptation to reservoir host immune systems, which were not already captured in estimation of reservoir host $T_w$ and $g_0$. $T_{vS}$ was thus computed as the inverse of the scaled time to most recent common ancestor (MRCA) for each mammalian reservoir host order from Primates (Fig. 3C; *SI Appendix,* Fig. S4, Table S1-S2), such that we estimated low human tolerance to viruses evolved in phylogenetically distant orders (e.g. monotreme and marsupial orders), and high human tolerance to viruses evolved in Primate and Primate-adjacent orders. In general, the modulating effects of $T_{vS}$ did little to alter virulence rankings of zoonotic viruses from those predicted by raw growth rate ($r_R^*$) alone—with the highest spillover virulence predicted from viruses evolved in orders Monotremata and Chiroptera and the lowest spillover virulence predicted from viruses evolved in orders Cetartiodactyla and Scandentia. Notably, modulating $T_{vS}$ enhanced predictions of spillover virulence for the marsupial clades (Peramelemorphia, Didelphimorphia, Dasyuromorphia, Diprotodontia) relative to eutherian orders with similar predicted $r_R^*$ values. This resulted in dampened predicted virulence for the eutherian order Cetartiodactyla as compared with marsupial orders Dasyuromorphia and Diprotodontia, despite lower predicted $r_R^*$ values (*SI Appendix,* Fig. S5).

***Comparing predictions of spillover virulence by reservoir order with estimates from the literature.***
Since parameter magnitudes estimated from life history traits were largely relative in nature, we scaled predictions of spillover virulence ($\alpha_S$) by reservoir order in relative terms to compare with estimates gleaned from the zoonosis literature (8) (Fig. 3D). Among the eight reservoir orders for which we were able to both generate nested modeling predictions and derive estimates from the literature (8), our nested modeling approach performed exceptionally well. Critically, we successfully recovered the key result from the zoonosis literature: bat-derived zoonoses yield higher rates of virus-induced mortality upon spillover to humans ($\alpha_S$) than do viruses derived from all other eutherian mammals (Fig. 3D; *SI Appendix,* Fig. S6-S7). In general, high estimates for $T_w$, $\mu$, and $g_0$ and low estimates for $T_{vS}$ predicted high spillover virulence to humans ($\alpha_S$). Bats demonstrate uniquely long lifespans for their body sizes and uniquely enhanced constitutive immune responses (21); when combined, as in our analysis, to represent high $T_w$ and high $g_0$, these reservoir host traits elevated predicted $r_R^*$ and $\alpha_S$ beyond all other eutherian orders. Evaluated against the data (8), our model underpredicted cross-order comparative virulence rankings for Carnivora-derived viruses, though the discrepancy in our predictions vs. those from the literature was somewhat resolved when rabies lyssavirus was excluded from data comparisons (*SI Appendix,* Fig. S7) (8). Though most rabies zoonoses are sourced from domestic dogs, lyssaviruses are Chiropteran by origin (54), and viral traits responsible for rabies' virulence may reflect its bat evolutionary history more than that of any intermediate carnivore host. Our model also successfully reproduced estimates of significantly lower virulence incurred by zoonotic viruses evolved in Cetartiodactyla hosts (8). While previous work suggested that this effect might result from overreporting of avirulent zoonoses in domestic livestock with frequent human contact (8), our analysis indicates that viral zoonoses emerging from Cetartiodactylan hosts may truly be less virulent to humans. Our mechanistic framework demonstrates that limited constitutive immune responses identified in Cetartiodactylan hosts may drive the evolution of low growth rate viruses that cause correspondingly benign infections following zoonotic emergence. Further research into the extent to which baseline neutrophil concentrations accurately reflect Cetartiodactylan innate immunity, as well as quantification of the natural growth rates of Cetartiodactylan viruses, is needed to evaluate the accuracy of these predictions.

## Discussion

Our work provides a mechanistic insight into the biological processes that underpin cross-species patterns in the evolution of virus virulence—a major advance for efforts to evaluate zoonotic risk. Using a simple model of evolving virus in a reservoir host immune system, we successfully recapture patterns previously reported in the literature that document both the distinctive virulence of viral zoonoses derived from bats and the surprising avirulence of viruses derived from Cetartiodactylan hosts (8). Additionally, our mechanistic approach allows us to make powerful predictions about the virulence of potential future viral spillovers, using general life history traits across mammals, including from orders for which zoonoses have not yet been reported (8). Our model indicates that we should anticipate the evolution of high growth rate viruses likely to cause virulence upon cross-species emergence from mammalian hosts with protracted lifespans for their body size (which we link to molecular mechanisms of immunopathological tolerance (49)), as well as from hosts with robust constitutive immune responses (34). While both immunopathological tolerance and constitutive immunity should drive the evolution of high growth rate viruses (Fig. 2), only tolerance will do so in the absence of reservoir host pathology, thus highlighting its selective influence in driving observed variation in the virulence of viral zoonoses. Importantly, while tolerance reduces pathogen-induced mortality for a single host, tolerant host populations (with limited checks on virus transmission) may demonstrate high pathogen prevalence. If imperfectly tolerant hosts still experience some virus-induced pathology, high prevalence can consequently elevate total population-level mortality for infected hosts—a phenomenon known as the 'tragedy of tolerance' (38, 39). Reports of virus-induced mortality in bats are rare (55), suggesting that bat virus tolerance is likely very effective.

Intriguingly, our independent evaluations of mammalian life history traits associated with enhanced longevity (a proxy for immunopathological tolerance (56, 57)) and robust constitutive immunity (48, 58) highlight several mammalian orders—chiefly Chiroptera and Monotremata—which show synergy in both features, offering support for ongoing efforts to elucidate links between anti-aging molecular pathways and antiviral immunity (52, 55). The order Cetartiodactyla presents a possible exception to this synergy that merits further study: on average, Cetartiodactylans demonstrate predictable lifespans per body size but significantly reduced constitutive immune responses as compared with other mammals. In all cases, predictions are limited by a dearth of comparative data in baseline immune cell concentrations across mammalian orders; notably, however, our estimation of enhanced constitutive immune responses in bats—derived from baseline neutrophil concentration for just ten species—is robustly supported by independent molecular work describing constitutive interferon expression in bat cells across multiple species (21, 59, 60).

Notably, we are able to recapture broad patterns in the literature while holding constant many basic immunological parameters—including rates of virus consumption by leukocytes ($c$), leukocyte activation upon viral infection ($g$), and reservoir host tolerance of direct virus pathology ($T_v$)—which almost certainly vary across taxa. Host tolerance of direct virus pathology, in particular, will likely also be modulated by virus tropism, offering another mechanism by which viral adaptation to reservoir hosts could enhance spillover virulence. For example, coronavirus tropism is thought to be localized largely in the gastrointestinal tract for bat hosts (61, 62): in our modeling framework, higher tolerance of direct virus pathology in this tissue should promote the evolution of higher growth rate viruses in bats, which are likely to cause virulence upon infection of more vulnerable tissues, such as the respiratory tract, in spillover hosts.

By summarizing within-host traits across mammalian orders, we generalize substantial within-clade diversity that likely contributes to heterogeneous patterns in available data. Bats alone make up more than 1,400 species and account for some 20% of mammalian diversity (63). Only a subset of bats are long-lived (64), and the magnitude of constitutive immunity is known to vary across bat species (21, 34, 42), suggesting considerable variation in the parameters $\mu$, $T_w$, and $g_0$, which we here model universally across the entire Chiropteran order. Thus, we can expect considerable variation in the evolution of virulence for viruses evolved in diverse species within a given order—which we largely disregard here. As more data becomes available, our modeling approach could be fine-tuned to make more specific, species-level predictions of highly virulent disease risk.

Our analysis does not consider the probability of cross species viral emergence, or the potential for onward transmission of a spilled-over virus in a human host—both of which have been shown to correlate

inversely with phylogenetic distance across mammals (4, 8, 9). Indeed, in keeping with trade-off theory, onward transmission of viruses following spillover is more commonly associated with low virulence infections (6, 8, 65, 66), suggesting that reservoir orders highlighted here as potential sources for high virulence pathogens are not necessarily the same orders likely to source future pandemics. Nonetheless, the possibility for virus adaptation to gain transmission advantages in human hosts following spillover—as witnessed for Ebola (67) and SARS-CoV-2 (68)—should not be ignored.

Currently, our work emphasizes the uniqueness of bats as flying mammals and, in consequence, as long-lived, tolerant reservoirs for highly virulent viral zoonoses. For the first time, we offer a mechanism for the evolution of bat-derived viruses that demonstrate significant pathology upon spillover to non-bat, particularly human, hosts. In providing a theoretical framework to explain this phenomenon, we generate a series of testable questions and hypotheses for future comparative immunological studies, to be carried out at *in vitro* and *in vivo* scales. Empirical work should aim to measure rates of immune cell activation, growth, and mortality across diverse mammalian orders and determine whether natural virus growth rates are truly higher when evolved in bat hosts. Additional studies should test whether anti-inflammatory mechanisms in bat cells of different tissues are equally effective at mitigating virus-induced pathology and immunopathology and whether comparative taxonomic predictions of virus tolerance, resistance, and virulence evolution apply to non-viral pathogens, too. In light of the emergence of SARS-CoV-2, the field of bat molecular biology has echoed the call for mechanistic understanding of bat immunology (69), and the NIH has responded (70), soliciting research on the development of tools needed to test the predictions outlined here. We offer a bottom-up mechanistic framework enabling the prediction of emerging virus virulence from the basic immunological and life-history traits of zoonotic hosts.

## Methods

### *Evolutionary framework.*

*Population-level dynamics.*

To evaluate the selective pressures that drive the evolution of cross-species virus virulence, we first sought to derive an equation for an optimal virus growth rate expressed in within-host parameters specific to the life history of the reservoir host. To this end, and in keeping with classic examples of viral maintenance in reservoir populations (71–77), we first modeled the dynamics of a persistent infection ($I_1$) in a hypothetical reservoir host, allowing for the introduction of a rare mutant virus strain which generates distinct infections in that same host ($I_2$) (see *SI Appendix* for more detailed methodology and derivations):

$$\frac{dS}{dt} = N(b - qN) - \beta_{r1}SI_1 - \beta_{r2}SI_2 - \mu S \qquad [1a]$$

$$\frac{dI_1}{dt} = \beta_{r1}SI_1 - \mu I_1 - \alpha_{r1}I_1 \qquad [1b]$$

$$\frac{dI_2}{dt} = \beta_{r2}SI_2 - \mu I_2 - \alpha_{r2}I_2 \qquad [1c]$$

Here, $N$ corresponds to the total host population and $S$ to all hosts susceptible to infection, such that $N = S + I_1 + I_2$. We assumed that hosts are born at rate $b$ and die of natural death at rate $\mu$, where $b > \mu$. We further assumed that all hosts are born susceptible and that population density is regulated via a crowding term ($q$). Because we aimed to model the evolution of rates that link to within-host dynamics for the reservoir host, we represented transmission and virulence as functions of the virus causing the infection (respectively, $\beta_r$ and $\alpha_r$) where $r$ denotes the intrinsic virus growth rate and is represented distinctly for both the endemic ($r_1$) and mutant ($r_2$) virus strains.

With the use of model [1], we performed an evolutionary invasion analysis (see *SI Appendix)* and concluded that the virus should evolve to maximize the ratio of transmission over infection duration. We refer to this ratio as the invasion fitness:

$$\frac{\beta_r}{\mu + \alpha_r} \qquad [2]$$

*Within-host dynamics.*

Next, to evaluate the within-host selective conditions underpinning the evolution of the virus growth rate ($r$), we sought to express the between-host parameters of transmission ($\beta_r$) and virulence ($\alpha_r$) in within-host terms, using a nested modeling approach. To this end, we established a simple within-host model representing the dynamics of infection *within* each $I_1$ and $I_2$ host as outlined above. We adapted a class of Lotka-Volterra predator-prey-like within-host models (reviewed in Alizon and van Baalen 2008 (78)), to overcome some constraints of basic predator-prey models of the immune system, chiefly *(i)* by allowing leukocytes to circulate in the absence of infection and *(ii)* by scaling leukocyte growth with virion density, independent of direct leukocyte-virion contact (79–81). This resulted in the following model, which demonstrates interactions between the virus population (V) and the leukocyte population (L) within each infected host:

$$\frac{dV}{dt} = rV - cVL \qquad [3a]$$

$$\frac{dL}{dt} = g_0 + grV - mL \qquad [3b]$$

Here, $r$ corresponds to the intrinsic virus growth rate, $c$ corresponds to the attack efficacy of the immune system upon contact with the virus, and $g$ signifies the recruitment rate of immune cells scaled to the virus growth rate. The parameter, $g_0$, describes the constitutive, baseline leukocyte recruitment in the absence of infection, and $m$ gives the natural leukocyte death rate.

Building from above, we expressed rates of population-level transmission and virulence known to depend on within-host dynamics ($\beta_{r1/r2}$ and $\alpha_{r1/r2}$) in terms of their within-host components, assuming that within-host dynamics are fast relative to host population-level dynamics and, therefore, converge to the endemic equilibrium (i.e. $mr > cg_0$).

In line with previous work, we assumed transmission to be a linear function of viral load (79), which we represented as:

$$\beta_r = \zeta V^*. \qquad [4]$$

where $\zeta$ corresponds to a scaling term equating viral load to transmission. We additionally assumed that:

$$\alpha_r = \frac{vrV^*}{T_v} + \frac{wgrV^*}{T_w}, \qquad [5]$$

by which infection-induced host mortality ('virulence') is modeled to result from both virus-induced pathology (a function of the intrinsic virulence of the parasite, $v$, and the parasite growth rate $rV^*$) and immunopathology—which we modeled as proportional to the leukocyte growth rate in response to virus expansion, multiplied by the host's susceptibility to immunopathology and inflammation ($w$). The terms $T_v$ and $T_w$ correspond to host tolerance of virus-induced pathology and immunopathology, respectively, under assumptions of "constant" tolerance, by which both virus pathology and immunopathology are reduced by a constant proportion across the course of infection. For constant tolerance, we assumed that $T_v > 1$ and $T_w > 1$. See *SI Appendix* for detailed derivations under assumptions of "complete" tolerance, whereby virus pathology and immunopathology are completely eliminated up to a threshold value, beyond which pathology scales proportionally with virus and immune cell growth.

Now, we rewrote the equations for transmission (*[4]*) and virulence (*[5]*) in purely within-host terms:

$$\beta_r = \frac{\zeta(mr - cg_0)}{cgr} \qquad [6]$$

$$\alpha_r = \frac{r(mr - cg_0)}{cgT_v} + \frac{w(mr - cg_0)}{cT_w} \qquad [7]$$

Using these within-host expressions, we then recomputed the expression for invasion fitness (*[2]*) in within host terms and determined the optimal intrinsic virus growth rate, which is an evolutionarily stable strategy (ESS) (see *SI Appendix)*:

$$r^* = \frac{cg_0}{m} + \frac{\sqrt{c^2m^2gg_0\mu T_vT_w(vT_w + gwT_v)}}{m^2(vT_w + gwT_v)} \qquad [8]$$

In Fig. 2, we explore the sensitivity of $r^*$, and the corresponding reservoir host population-level transmission ($\beta^*$) and virulence ($\alpha^*$) at that growth rate, across varied values for its within-host component parameters.

*Cross-species dynamics.*

We next sought to derive an expression to explore the consequences of spillover of a virus evolved to its optimal growth rate in a reservoir host population – which we termed $r_R^*$ – following cross-species emergence into the human population. Contrary to its established persistent infection in the reservoir host, we assumed that such a virus would produce an acute infection in the spillover host. To model the dynamics of this acute spillover, we borrowed from Gilchrist and Sasaki 2002 (82), who developed a within-host parasite-leukocyte model in which an immortal leukocyte successfully eradicates the parasite population to near-zero. We modified their acute model to be more comparable to our chronic infection model (*[3a]/[3b])* and to reflect our differing notation for within-host dynamics.

$$\frac{dV_S}{d\tau} = r_R^*V_S - c_SV_SL_S \qquad [9a]$$

$$\frac{dL_S}{d\tau} = r_R^*g_SV_S \qquad [9b]$$

Here, $r_R^*$ represents the reservoir-evolved virus growth rate, but all other terms reflect within-host conditions of the spillover host: $V_S$ and $L_S$ correspond, respectively, to the spillover host virus and leukocyte populations, $c_S$ is the virus consumption rate upon contact with leukocytes in the spillover host,

and $g_S$ is the growth rate of the spillover host leukocyte population in response to virus. We expressed the model in units of $\tau$, which we assume to be short in comparison to the $t$ time units of dynamics in the reservoir host population. Rather than solving for virus and leukocyte populations at equilibrium (as in the reservoir host population), we instead derived an expression for the virus population at the peak of infection ($V_{S_{max}}$), where we anticipated maximum pathology for the spillover host.

To achieve this, we divided equation *[9a]* by equation *[9b]* to derive a simple, time-independent solution demonstrating the relationship between virus and leukocyte density:

$$\frac{dV_S}{dL_S} = \frac{1}{g_S}\left(1 - \frac{c_S L_S}{r_R^*}\right) \qquad [10]$$

Integration of *[10]* established the following relationship between virus and leukocyte:

$$V_S = \frac{1}{g_S} L_S - \frac{c_S}{2r_R^* g_S}(L_S)^2 + 1 - \frac{1}{g} + \frac{c_S}{2r_S^* g_S} \qquad [11]$$

We let $L_S(0) = 1, V_S(0) = 1$, since both virus and leukocyte populations were assumed to be small at $\tau = 0$. Using equation *[11],* we were then able to derive an expression for $V_{S_{max}}$, the maximum viral load, which should precede the end of acute infection and the point of host recovery at the maximum age of infection:

$$V_{S_{max}} = \frac{r_R^*}{g_S c_S} - \frac{r_R^*}{2g_S c_S} + 1 - \frac{1}{g_S} + \frac{c_S}{2r_R^* g_S} \qquad [12]$$

Now that we had an established expression for $V_{S_{max}}$, we adapted equation *[7]* to reflect the acute within-host dynamics of "spillover virulence", which we modeled (as before) as a combination of mortality induced from direct virus pathology and from immunopathology. The virulence of the virus in the spillover host will vary with time, $\tau$, tracking the within-host viral load in that same host ($V_S(\tau)$) but should be highest at peak viral load ($V_{S_{max}}$). As in the reservoir host system, we also modeled the mitigating impact of tolerance on the two mechanisms of virulence:

$$\alpha_S = V_{S_{max}}\left(\frac{r_R^* v}{T_{vS}(\eta_R)} + \frac{g_S w_S r_R^*}{T_{wS}}\right) \qquad [13]$$

This yielded the above expression for 'spillover virulence'. Here, the growth rate of the virus is expressed at its evolutionary optimum evolved in the reservoir host ($r_R^*$), and the virus's intrinsic virulence ($v$) is unchanged from one host to the next. Inspired by findings in the literature that report higher virulence in cross-species infections between hosts separated by larger phylogenetic distances (8–12), we modeled spillover host tolerance of virus-induced pathology ($T_{vS}$) as a decreasing function of increasing phylogenetic distance between the reservoir and secondary host, here given as $\eta_R$. All other immune-related parameters took on characteristics of the spillover host: $g_S$ is the spillover host's leukocyte growth rate, $w_S$ is the spillover host's susceptibility to immunopathology and inflammation, and $T_{wS}$ corresponds to the spillover host's tolerance of immunopathology.

***Order-specific estimates for optimal virus growth rates evolved in reservoir hosts.***

Next, we sought to develop estimates for the optimal virus growth rate ($r_R^*$) expected to evolve across a suite of diverse mammalian reservoir orders. Because within-host immunological data needed to quantify within-host parameters underpinning the expression for $r_R^*$ are largely lacking, we chose to proxy a few key within-host parameters from well-described allometric relationships for mammalian life history data. As such, we here focus on three key parameters for which data could be gleaned from the literature: the reservoir host mortality rate ($\mu$), the reservoir host tolerance of immunopathology ($T_w$), and the magnitude of reservoir host constitutive immunity ($g_0$).

To generate order-level summary terms for $\mu$ and $T_w$, we fit a generalized additive model (44) using the 'mgcv' package in R to the relationship between $\log_{10}$ adult body mass (in g) and $\log_{10}$ maximum life span

(in years). We fit our GAM to data from Jones et al. 2009 (56) and Healy et al. 2014 (57), incorporating a random effect of mammalian order (*SI Appendix,* Table S2). Mass and lifespan data (Fig. 3A) spanned 26 mammalian orders and 1055 individual species. In lieu of phylogeny, we incorporated a random effect of mammalian host order in all GAMs, which enabled us to produce order-level summary terms for each parameter. To estimate $\mu$, we predicted maximum lifespan by mammalian order from the fitted GAM using the predict.gam function in 'mgcv', while excluding the effects of adult body mass, then took the inverse of that prediction to obtain an estimate of order-level annual mortality (*SI Appendix,* Table S1). To estimate $T_w$, we extracted the relative partial effects of mammalian order on maximum lifespan, then rescaled these effects between 1 and 2 for assumptions of constant tolerance and between 0 and 1 for assumptions of complete tolerance. We justify this approach based on literature that highlights links between anti-aging molecular pathways that promote longevity and those that mitigate immunopathology (11, 42, 50–53). Thus, order-level estimates for $\mu$ and $T_w$ are relative inverses of one another, as highlighted in *SI Appendix*, Fig. S4 (Table S1).

To generate order-level summary terms for the magnitude of constitutive immunity ($g_0$), we fit a GAM to the relationship between the predictor variables of $\log_{10}$ mass (in g) and basal metabolic rate (BMR, in W) and the response variable of $\log_{10}$ baseline neutrophil concentration (in $10^9$ cells/L), which offers an approximation of a mammal's constitutive innate immune response. BMR data for this model were derived from Jones et al. 2009 (56) and Healy et al. 2014 (57), while neutrophil concentrations were obtained from zoo animal data presented in the Species360 database (49); prior work using this database has demonstrated scaling relationships between body size and immune cells across mammals (48). Paired neutrophil and BMR data were limited to just 19 mammalian orders and 144 species. Our GAM included a random effect of host order (in lieu of 'phylogeny', the significant predictor used in the original authors' models) and revealed a statistically significant effect of host order modulating the relationship between body mass, BMR, and neutrophil concentration. Using a similar approach as that employed above for $T_w$, we estimated $g_0$ by extracting the relative partial effects of mammalian order on neutrophil concentration, then rescaled these effects between 0 and 1. Because we estimated significantly positive partial effects between the orders Chiroptera and Monotremata and baseline neutrophil concentration (Fig. S3), this generated correspondingly high estimates of $g_0$ for these two orders (Fig. S4, Table S3).

Using these order-level summary terms for $\mu$, $T_w$, and $g_0$, we then generated an order-level prediction for $r_R^*$ across all mammalian host orders, following equation *[8]* (*SI Appendix,* Fig. S5). All other parameters ($c$, $g$, $m$, $w$, $v$, and $T_v$) were held constant across all taxa at values listed in Table 1.

***Estimating zoonotic virus virulence in spillover human hosts.***

Once we had constructed an order-level prediction for $r_R^*$, we finally sought to explore the effects of these reservoir-evolved viruses upon spillover to humans, following equation *[13].* As when computing virulence for the reservoir host population, we held immunological parameters, $c$, $g$, $m$, and $w$, constant in humans (at the same values listed above) due to a lack of informative data to the contrary. Then, to generate an order-level estimate for virus virulence incurred on humans ($\alpha_S$), we combined our order-level predictions for $r_R^*$ with order-specific values for $T_{vS}$, the human tolerance of an animal-derived virus, which we scaled such that viruses derived from more closely-related orders to Primates were more easily tolerated in humans. Specifically, we represented $T_{vS}$ as the scaled inverse of $\eta_R$, the cophenetic phylogenetic distance of each mammalian order from Primates. No summarizing was needed for $\eta_R$ because, following Mollentze and Streicker 2020 (10), we used a composite time-scaled reservoir phylogeny derived from the TimeTree database (83), which produced a single mean divergence date for all clades. Thus, all species within a given mammalian order were assigned identical times to most recent common ancestor with the order Primates. To convert $\eta_R$ to reasonable values for $T_{vS}$, we divided all order-level values of $\eta_R$ by the largest (to generate a fraction), then subtracted that fraction from 2 for assumptions of constant tolerance (yielding $T_{vS}$ estimates ranging from 1-2) and from 1 for assumptions of complete tolerance (yielding $T_{vS}$ estimates ranging from 0-1).

We then combined reservoir host order-level predictions for $r_R^*$ with these estimates for human tolerance of virus pathology ($T_{vS}$) to generate predictions of the expected spillover virulence of viral zoonoses emerging from the 19 mammalian orders for which we possessed complete data across the four variable

parameters ($\mu$, $T_w$, $g_0$, and $T_{vS}$). We scaled these $\alpha_S$ estimates—and their 95% predicted confidence intervals—in relative terms (from 0 to 1) to compare with estimates from the literature.

***Comparing predictions of spillover virulence by reservoir order with estimates from the literature.*** To compare estimates of spillover virulence generated from our nested modeling approach ($\alpha_S$) with estimates from the literature, we next followed Day 2002 (84) to convert case fatality rates of viral zoonoses in spillover human hosts ($CFR_S$) reported in the literature (8) to empirical estimates of $\alpha_S$ for each mammalian order, using data on the duration of human infection ($D_{IS}$) for each viral zoonosis. For this purpose, we collected $D_{IS}$ ourselves by searching the primary literature; raw data for infection durations and associated references are reported in our publicly available GitHub repository. Briefly, Day 2002 (13) notes that the equation for case fatality rate in the spillover host ($CFR_S$) takes the form:

$$CFR_S = \frac{\alpha_S}{\alpha_S + \sigma_S} \qquad [14]$$

where $\sigma_S$ corresponds to the recovery rate from the spilled-over-virus in the human host. We also note that the total duration of infection, $D_{IS}$, is given by:

$$D_{IS} = \frac{1}{\alpha_S + \sigma_S} \qquad [15]$$

Therefore, we translated human case fatality rates of viral zoonoses ($CFR_S$) into estimates of spillover virulence ($\alpha_S$) using the following equation:

$$\alpha_S = \frac{CFR_S}{D_{IS}} \qquad [16]$$

To obtain a composite order-level prediction for $\alpha_S$ from $D_{IS}$ and $CFR_S$ as reported in (8), we adopted the best-fit GAM used by the authors in (8) to summarize $CFR_S$ by order and, here, applied it to $\alpha_S$ estimates converted from $CFR_S$ reported in the literature (*SI Appendix,* Table S2). We then summarized $\alpha_S$ at the order-level from the fitted GAM, excluding the effects of viral family. This yielded a literature-derived value for $\alpha_S$ across disparate mammalian orders, against which to compare predictions from our nested modeling approach. Because the majority of the within-host parameters underpinning $\alpha_S$ predictions in our nested modeling approach ($\mu$, $T_w$, $g_0$, and $T_{vS}$) were quantified only in a relative fashion, we were unable to compare direct magnitudes of virulence (e.g. in terms of host death per unit time). To account for this, we rescaled $\alpha_S$ estimates from both our nested modeling approach and from the empirical literature from 0 to 1 and compared the relative rank of virulence by mammalian order instead. We predicted $\alpha_S$ for 19 discrete mammalian orders, though data from the literature were available for only 8 orders against which to compare.

Finally, because bats are the most likely ancestral hosts of all lyssaviruses (54), and it may be more appropriate to class carnivores as 'bridge hosts' for rabies, rather than reservoirs (as the authors discuss in Guth et al. 2022 (8)), we recomputed literature-derived estimates of relative $\alpha_S$ by fitting the same GAMs (*SI Appendix,* Table S2) to a version of the dataset excluding all entries for rabies lyssavirus. We rescaled these new estimates of spillover virulence between 0 and 1 and compared them again to predictions from our nested modeling approach in *SI Appendix,* Fig. S6-S7.

**Data availability:**

All raw data and corresponding code for analysis and modeling are publicly available at the following GitHub repository: github.com/brooklabteam/spillover-virulence

**Acknowledgments**

The authors thank the Boots Lab at UC Berkeley for helpful comments on this manuscript and acknowledge funding from a National Institutes of Health grant (1R01AI129822-01) to CEB, an Adolph C. and Mary Sprague Miller Institute for Basic Research fellowship to CEB, a Branco Weiss Science in Society fellowship to CEB, a AAAS/Loréal-USA for Women in Science fellowship to CEB, and a Defense Advanced Research Projects Agency PREEMPT Program subgrant (D18AC00031) to CEB.

## References


1. C. Bonneaud, B. Longdon, Emerging pathogen evolution. *EMBO Reports* **21**, e51374 (2020).
2. J.-B. André, M. E. Hochberg, Virulence evolution in emerging infectious diseases. *Evolution* **59**, 1406 (2005).
3. B. M. Bolker, A. Nanda, D. Shah, Transient virulence of emerging pathogens. *Journal of the Royal Society Interface* **7**, 811–822 (2010).
4. S. Guth, E. Visher, M. Boots, C. E. Brook, Host phylogenetic distance drives trends in virus virulence and transmissibility across the animal – human interface. *Phil. Trans. R. Soc B* **374**, 20190296 (2019).
5. M. J. Farrell, T. J. Davies, Disease mortality in domesticated animals is predicted by host evolutionary relationships. *Proceedings of the National Academy of Sciences of the United States of America* **116**, 7911–7915 (2019).
6. N. Mollentze, D. G. Streicker, P. R. Murcia, K. Hampson, R. Biek, Virulence mismatches in index hosts shape the outcomes of cross-species transmission. *Proceedings of the National Academy of Sciences of the United States of America* (2020) https:/doi.org/10.1073/pnas.2006778117.
7. B. Longdon, *et al.*, The causes and consequences of changes in virulence following pathogen host shifts. *PLoS Pathog* **11**, e1004728 (2015).
8. S. Guth, *et al.*, Bats host the most virulent—but not the most dangerous—zoonotic viruses. *Proc. Natl. Acad. Sci. U.S.A.* **119**, e2113628119 (2022).
9. K. J. Olival, *et al.*, Host and viral traits predict zoonotic spillover from mammals. *Nature* (2017) https:/doi.org/10.1038/nature22975.
10. N. Mollentze, D. G. Streicker, Viral zoonotic risk is homogenous among taxonomic orders of mammalian and avian reservoir hosts. *Proceedings of the National Academy of Sciences*, 1–8 (2020).
11. A. T. Irving, M. Ahn, G. Goh, D. E. Anderson, L.-F. Wang, Lessons from the host defences of bats, a unique viral reservoir. *Nature* **589**, 363–370 (2021).
12. T. Schountz, M. L. Baker, J. Butler, V. Munster, Immunological control of viral infections in bats and the emergence of viruses highly pathogenic to humans. *Frontiers in Immunology* **8**, 1098 (2017).
13. M. Boots, Fight or learn to live with the consequences. *Trends in Ecology and Evolution* **23**, 245–248 (2008).
14. L. Råberg, D. Sim, A. F. Read, Disentangling genetic variation for resistance and tolerance to infectious diseases in animals. *Science* **318**, 812–814 (2007).
15. L. Råberg, A. L. Graham, A. F. Read, Decomposing health: tolerance and resistance to parasites in animals. *Philosophical transactions of the Royal Society of London. Series B, Biological sciences* **364**, 37–49 (2009).
16. S. Mougari, C. Gonzalez, O. Reynard, B. Horvat, Fruit bats as natural reservoir of highly pathogenic henipaviruses: balance between antiviral defense and viral tolerance. *Current Opinion in Virology* **54**, 101228 (2022).
17. M. Ng, *et al.*, NPC1 contributes to species-specific patterns of Ebola virus infection in bats. *eLife* **4**, e11785 (2015).
18. T. N. Starr, *et al.*, ACE2 binding is an ancestral and evolvable trait of sarbecoviruses. *Nature* **603**, 913–918 (2022).
19. M. Letko, *et al.*, Adaptive evolution of MERS-CoV to species variation in DPP4. *Cell Reports* **24**, 1730–1737 (2018).
20. M. Letko, A. Marzi, V. Munster, Functional assessment of cell entry and receptor usage for SARS-CoV-2 and other lineage B betacoronaviruses. *Nature Microbiology* **5**, 562–569 (2020).
21. P. Zhou, *et al.*, Contraction of the type I IFN locus and unusual constitutive expression of IFN-α in bats. *Proceedings of the National Academy of Sciences* **113**, 2696–2701 (2016).
22. E. D. Laing, *et al.*, Enhanced autophagy contributes to reduced viral infection in black flying fox cells. *Viruses* **11** (2019).
23. Y. T. Chionh, *et al.*, High basal heat-shock protein expression in bats confers resistance to cellular heat/oxidative stress. *Cell Stress and Chaperones* **24**, 835–849 (2019).
24. T. J. O'Shea, *et al.*, Bat flight and zoonotic viruses. *Emerging Infectious Diseases* **20**, 741–745 (2014).

25. B. Y. S. P. Thomas, R. A. Suthers, The physiology and energetics of bat flight. *Journal of Experimental Biology* **57**, 317–335 (1972).
26. J. Speakman, D. Thomas, “Physiological ecology and energetics of bats” in *Bat Ecology*, T. Kunz, M. Fenton, Eds. (University of Chicago Press, 2003), pp. 430–490.
27. G. Zhang, *et al.*, Comparative analysis of bat genomes provides insight into the evolution of flight and immunity. *Science* **339**, 456–60 (2013).
28. D. M. Santillan, *et al.*, Large-scale genome sampling reveals unique immunity and metabolic adaptations in bats. *Molecular Ecology* (2021) https:/doi.org/10.1111/mec.16027.
29. M. Ahn, J. Cui, A. T. Irving, L.-F. Wang, Unique loss of the PYHIN gene family in bats amongst mammals: Implications for inflammasome sensing. *Scientific Reports* **6**, 21722 (2016).
30. M. Ahn, *et al.*, Dampened NLRP3-mediated inflammation in bats and implications for a special viral reservoir host. *Nature Microbiology* **4** (2019).
31. J. Xie, *et al.*, Dampened STING-dependent interferon activation in bats. *Cell Host and Microbe* **23**, 1–5 (2018).
32. G. Goh, *et al.*, Complementary regulation of caspase-1 and IL-1 β reveals additional mechanisms of dampened inflammation in bats. *Proceedings of the National Academy of Sciences* (2020) https:/doi.org/10.1073/pnas.2003352117.
33. S. N. Austad, K. E. Fischer, Mammalian aging, metabolism, and ecology: evidence from the bats and marsupials. *Journal of gerontology* **46**, B47-53 (1991).
34. C. E. Brook, *et al.*, Accelerated viral dynamics in bat cell lines, with implications for zoonotic emergence. *eLife* **9**, e48401 (2020).
35. D. Ebert, J. J. Bull, Challenging the trade-off model for the evolution of virulence: is virulence management feasible? *Trends in Microbiology* **11**, 15–20 (2003).
36. S. Alizon, A. Hurford, N. Mideo, M. Van Baalen, Virulence evolution and the trade-off hypothesis: History, current state of affairs and the future. *Journal of Evolutionary Biology* **22**, 245–259 (2009).
37. R. M. Anderson, R. M. May, Coevolution of hosts and parasites. *Parasitology* **85**, 411–426 (1982).
38. M. R. Miller, A. White, M. Boots, The evolution of parasites in response to tolerance in their hosts: The good, the bad, and apparent commensalism. *Evolution* **60**, 945 (2006).
39. A. Best, A. White, M. Boots, The coevolutionary implications of host tolerance. *Evolution* **68**, 1426–1435 (2014).
40. H. E. Randolph, L. B. Barreiro, Holy Immune Tolerance, Batman! *Immunity* **48**, 1074–1076 (2018).
41. D. T. S. Hayman, Bat tolerance to viral infections. *Nature Microbiology* **4**, 728–729 (2019).
42. S. S. Pavlovich, *et al.*, The Egyptian Rousette genome reveals unexpected features of bat antiviral immunity. *Cell* **173**, 1–13 (2018).
43. S. A. H. Geritz, É. Kisdi, G. Meszéna, J. A. J. Metz, Evolutionarily singular strategies and the adaptive growth and branching of the evolutionary tree. *Evolutionary Ecology* **12**, 35–57 (1998).
44. S. N. Wood, mgcv: GAMs and Generalized Ridge Regression for R. *R News* **1/2**, 20–24 (2001).
45. Brown, James, West, Geoffrey, Enquist, Brian, “Scaling in biology: Patterns and processes, causes and consequences” in *Scaling in Biology*, (Oxford University Press, 2000), pp. 87–112.
46. J. H. Brown, J. F. Gillooly, A. P. Allen, V. M. Savage, G. B. West, Towards a metabolic theory of ecology. *Ecology* **85**, 1771–1789 (2004).
47. G. B. West, W. H. Woodruff, J. H. Brown, Allometric scaling of metabolic rate from molecules and mitochondria to cells and mammals. *Proceedings of the National Academy of Sciences of the United States of America* **99**, 2473–2478 (2002).
48. C. J. Downs, N. A. Dochtermann, R. Ball, K. C. Klasing, L. B. Martin, The effects of body mass on immune cell concentrations of mammals. *American Naturalist* **195**, 107–114 (2020).
49. Species360 Zoological Information Management System (ZIMS) (August 25, 2022).
50. G. S. Wilkinson, *et al.*, DNA methylation predicts age and provides insight into exceptional longevity of bats. *Nature Communications* **12** (2021).
51. J. Dhinaut, A. Balourdet, M. Teixeira, M. Chogne, Y. Moret, A dietary carotenoid reduces immunopathology and enhances longevity through an immune depressive effect in an insect model. *Scientific Reports* **7** (2017).
52. C. Caruso, D. Lio, L. Cavallone, Aging, longevity, inflammation, and cancer. *Annals of New York Academiy of Sciences* **1028**, 1–13 (2004).
53. D. K. Fabian, *et al.*, Evolution of longevity improves immunity in *Drosophila*. *Evolution Letters* **2**, 567–579 (2018).

54. C. E. Rupprecht, A. Turmelle, I. V. Kuzmin, A perspective on lyssavirus emergence and perpetuation. *Current Opinion in Virology* **1**, 662–670 (2016).
55. C. E. Brook, A. P. Dobson, Bats as 'special' reservoirs for emerging zoonotic pathogens. *Trends in Microbiology* **23**, 172–80 (2015).
56. K. E. Jones, *et al.*, PanTHERIA: a species-level database of life history, ecology, and geography of extant and recently extinct mammals. *Ecology* **90**, 2648–2648 (2009).
57. K. Healy, *et al.*, Ecology and mode-of-life explain lifespan variation in birds and mammals. *Proceedings of the Royal Society B* (2014).
58. R. Hamilton, M. Siva-Jothy, M. Boots, Two arms are better than one: Parasite variation leads to combined inducible and constitutive innate immune responses. *Proceedings of the Royal Society B: Biological Sciences* **275**, 937–945 (2008).
59. A. E. Shaw, *et al.*, Fundamental properties of the mammalian innate immune system revealed by multispecies comparison of type I interferon responses. *PLoS Biol* **15**, e2004086 (2017).
60. E. Clayton, M. Munir, Fundamental characteristics of bat interferon systems. *Front. Cell. Infect. Microbiol.* **10**, 527921 (2020).
61. W. Widagdo, *et al.*, Tissue distribution of the MERS-coronavirus receptor in bats. *Sci Rep* **7**, 1193 (2017).
62. M. Ruiz-Aravena, *et al.*, Ecology, evolution and spillover of coronaviruses from bats. *Nature Reviews Microbiology* (2021) https:/doi.org/10.1038/s41579-021-00652-2.
63. N. Simmons, A. Cirranello, Bat species of the world: A taxonomic and geographic database (2020) (July 11, 2020).
64. G. S. Wilkinson, D. M. Adams, Recurrent evolution of extreme longevity in bats. *Biology Letters* **15**, 20180860 (2019).
65. J. L. Geoghegan, A. M. Senior, F. Di, E. C. Holmes, Virological factors that increase the transmissibility of emerging human viruses. *Proceedings of the National Academy of Sciences* **113**, 4170–4175 (2016).
66. B. Longdon, J. D. Hadfield, C. L. Webster, D. J. Obbard, F. M. Jiggins, Host phylogeny determines viral persistence and replication in novel hosts. *PLoS Pathogens* **7** (2011).
67. R. A. Urbanowicz, *et al.*, Human adaptation of Ebola virus during the West African Outbreak. *Cell* **167**, 1079–1087 (2016).
68. J. A. Plante, *et al.*, Spike mutation D614G alters SARS-CoV-2 fitness. *Nature* (2020) https:/doi.org/10.1038/s41586-020-2895-3.
69. L.-F. Wang, A. M. Gamage, W. O. Y. Chan, Decoding bat immunity: the need for a coordinated research approach. *Nature Reviews Immunology* **0123456789**, 0–2 (2021).
70. National Institutes of Health, Research on Bat Immunology.
71. M. Viana, *et al.*, Assembling evidence for identifying reservoirs of infection. *Trends in Ecology and Evolution* **29**, 270–9 (2014).
72. K. Hampson, D. T. Haydon, Persistent pathogens and wildlife reservoirs. *Science* **374**, 35–36 (2021).
73. D. T. Haydon, S. Cleaveland, L. H. Taylor, M. K. Laurenson, Identifying reservoirs of infection: A conceptual and practical challenge. *Emerging infectious diseases* **8**, 1468–73 (2002).
74. A. Jolles, *et al.*, Endemic persistence of a highly contagious pathogen: Foot-and-mouth disease in its wildlife host. *Science* **374**, 104–109 (2021).
75. R. K. Plowright, *et al.*, Transmission or within-host dynamics driving pulses of zoonotic viruses in reservoir-host populations. *PLoS Neglected Tropical Diseases* **10**, e0004796 (2016).
76. T. Schountz, *et al.*, Regulatory T cell-like responses in deer mice persistently infected with Sin Nombre virus. *Proceedings of the National Academy of Sciences* **104**, 15496–15501 (2007).
77. T. Schountz, J. Prescott, Hantavirus immunology of rodent reservoirs: Current status and future directions. *Viruses* **6**, 1317–1335 (2014).
78. S. Alizon, M. van Baalen, Acute or Chronic? Within-host models with immune dynamics, infection outcome, and parasite evolution. *The American Naturalist* **172**, E244–E256 (2008).
79. S. Alizon, M. van Baalen, Emergence of a convex trade-off between transmission and virulence. *The American Naturalist* **165**, E155–E167 (2005).
80. S. Alizon, M. van Baalen, Multiple infections, immune dynamics, and the evolution of virulence. *The American Naturalist* **172**, E150–E168 (2008).

81. A. Fenton, J. Lello, M. B. Bonsall, Pathogen responses to host immunity: The impact of time delays and memory on the evolution of virulence. *Proceedings of the Royal Society B: Biological Sciences* **273**, 2083–2090 (2006).
82. M. A. Gilchrist, A. Sasaki, Modeling host – parasite coevolution: A nested approach based on mechanistic models. *Journal of Theoretical Biology* **218**, 289–308 (2002).
83. S. Kumar, G. Stecher, M. Suleski, S. B. Hedges, TimeTree: a resource for timelines, timetrees, and divergence times. *Molecular Biology and Evolution* **34**, 1812–1819 (2017).
84. T. Day, On the evolution of virulence and the relationship between various measures of mortality. *Proceedings of the Royal Society B* **269**, 1317–1323 (2002).
85. M. Boots, R. Donnelly, A. White, Optimal immune defence in the light of variation in lifespan. *Parasite Immunology* **35**, 331–338 (2013).

**Table 1. Default parameter values for population-level and within-host models.**

| Parameter | Definition | Units | Value* | Scale |
|---|---|---|---|---|
| $\boldsymbol{b}$ | host natural birth rate | days$^{-1}$ | $0.2$ | population-level |
| $\boldsymbol{q}$ | crowding term to regulate density-dependent growth | days$^{-1}$ | $0.0002$ | population-level |
| $\boldsymbol{\mu}^{\dagger}$ | host background mortality rate | days$^{-1}$ | $\frac{1}{20 * 365}$ | population-level |
| $\boldsymbol{g_0}^{\dagger}$ | magnitude of constitutive immunity *(rate of baseline neutrophil supply)* | days$^{-1}$ | .3 | within-host |
| $\boldsymbol{g}$ | rate of leukocyte activation by virus | days$^{-1}$ | $0.9$ | within-host |
| $\boldsymbol{c}$ | rate of virus consumption by leukocyte | days$^{-1}$ | $0.5$ | within-host |
| $\boldsymbol{m}$ | background mortality rate for leukocytes | days$^{-1}$ | $\frac{1}{21}$ | within-host |
| $\boldsymbol{\zeta}$ | maximum between-host transmission rate | days$^{-1}$ | $0.2$ | within-host |
| $\boldsymbol{w}$ | host susceptibility to immunopathology | leukocytes$^{-1}$ | $1$ | within-host |
| $\boldsymbol{v}$ | intrinsic virus virulence | virions$^{-1}$ | $1$ | within-host |
| $\boldsymbol{T_w}^{\dagger}$ | tolerance of immunopathology (constant or complete) | unitless | *variable*<br>constant: $1-2$<br>complete: $0-1$ | within-host |
| $\boldsymbol{T_{vS}}^{\dagger}$ | human tolerance of viral pathology (constant or complete) | unitless | *variable*<br>constant: $1-2$<br>complete: $0-1$ | between-host spillover |

*Value column gives parameter values fixed in Fig. 2 and *SI Appendix,* Fig. S2, excepting instances when parameter was modulated along the x-axis or internally ($T_w$, $T_v$) as indicated in the figure legend. Parameter values are comparable to the ranges explored in Miller et al. 2006 (38) and Boots et al. 2013 (85).
$^{\dagger}$Parameters $\mu$, $g_0$ ,$T_w$, and $T_{vS}$ were modeled as functions of mammalian order-specific life history traits in Fig. 3 and in *SI Appendix,* Fig. S6-S7, as outlined in the Methods.

1037

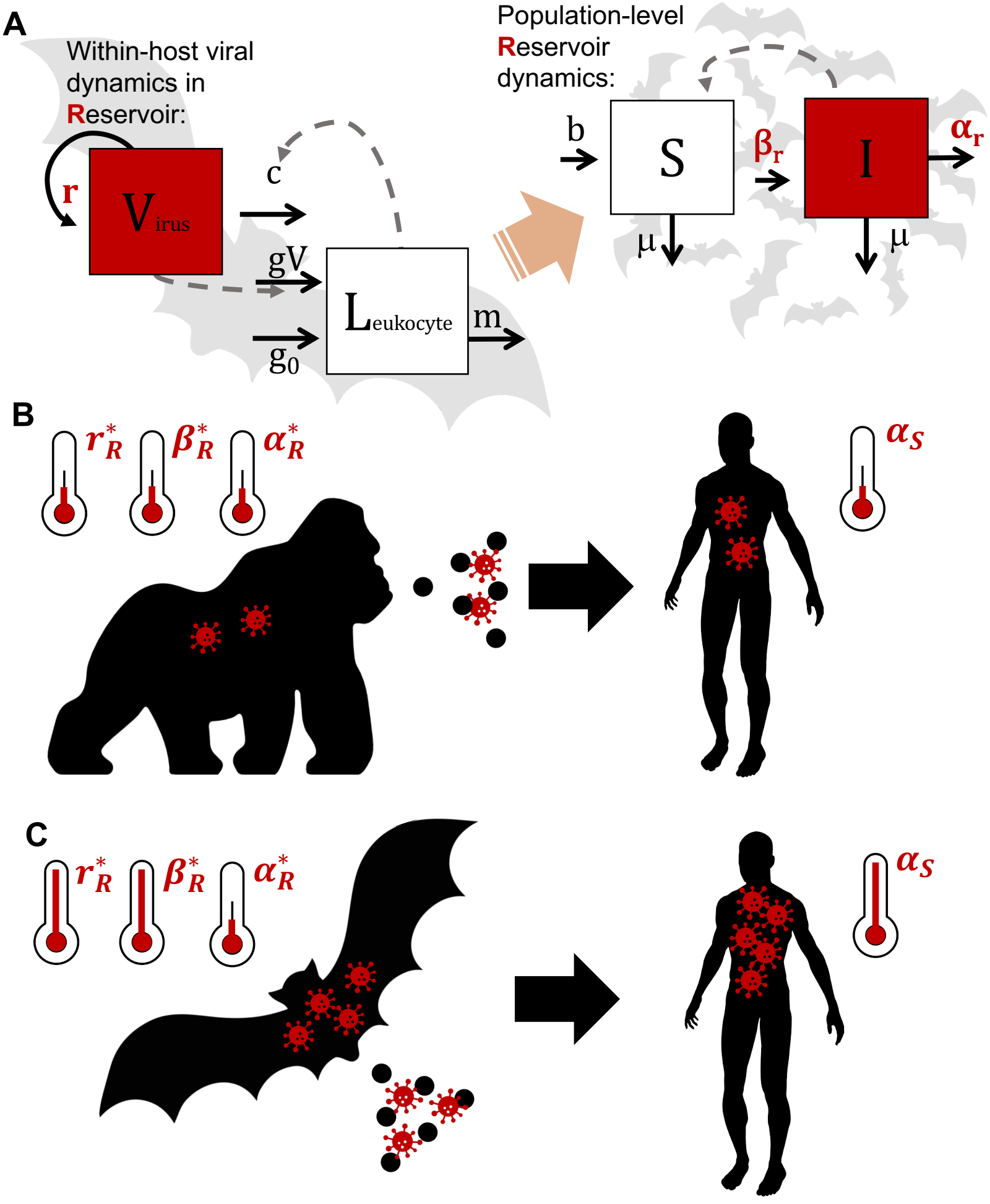
A
Within-host viral dynamics in Reservoir:
r
Virus
c
gV
g0
Leukocyte
m
Population-level Reservoir dynamics:
b
S
βr
I
αr
μ
μ
B
$r_R^*$
$\beta_R^*$
$\alpha_R^*$
$\alpha_S$
C
$r_R^*$
$\beta_R^*$
$\alpha_R^*$
$\alpha_S$

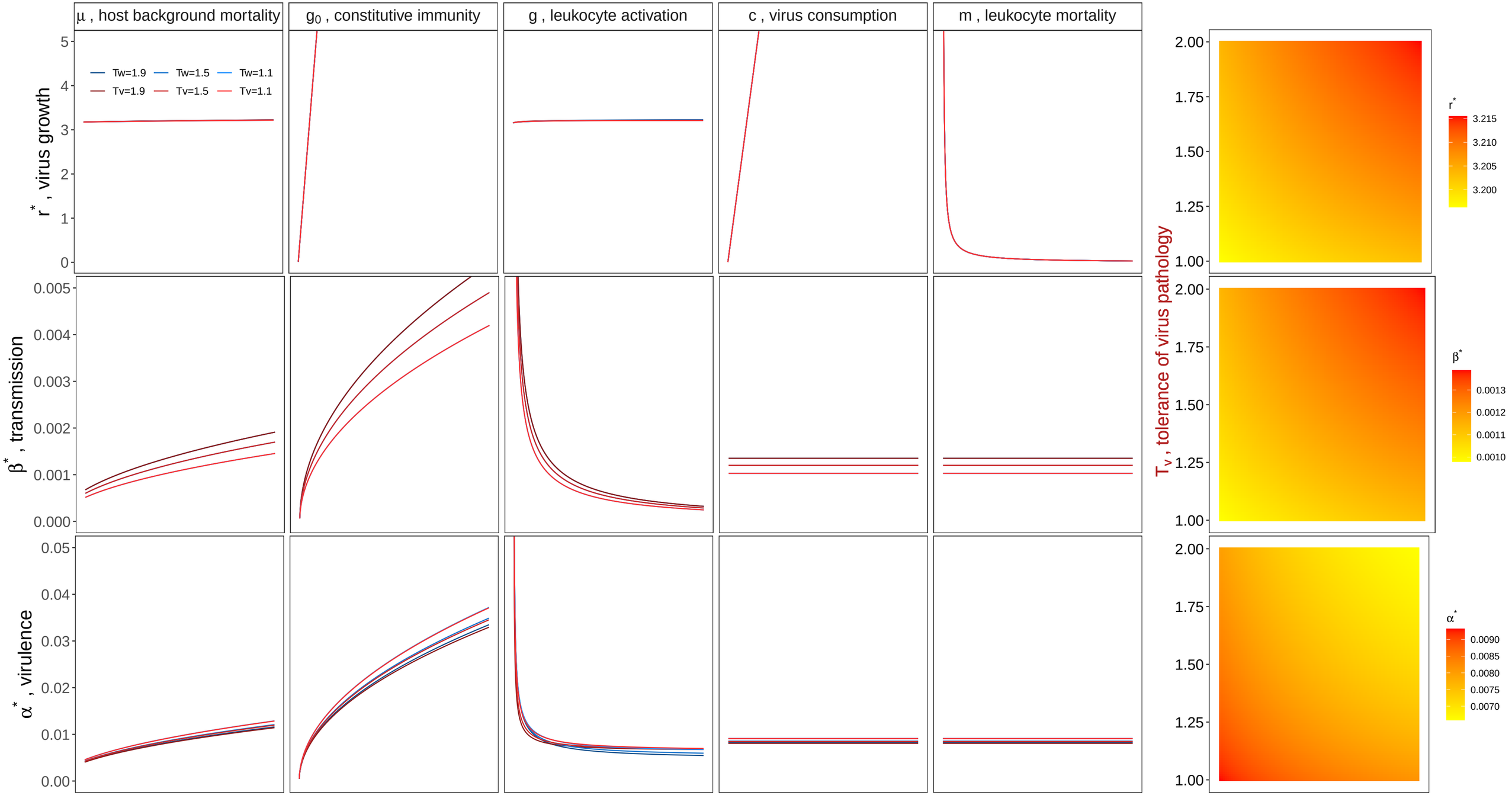
μ , host background mortality
g0 , constitutive immunity
g , leukocyte activation
c , virus consumption
m , leukocyte mortality
Tw=1.9
Tw=1.5
Tw=1.1
Tv=1.9
Tv=1.5
Tv=1.1
r* , virus growth
β* , transmission
α* , virulence
Tv , tolerance of virus pathology
r*
3.215
3.210
3.205
3.200
β*
0.0013
0.0012
0.0011
0.0010
α*
0.0090
0.0085
0.0080
0.0075
0.0070

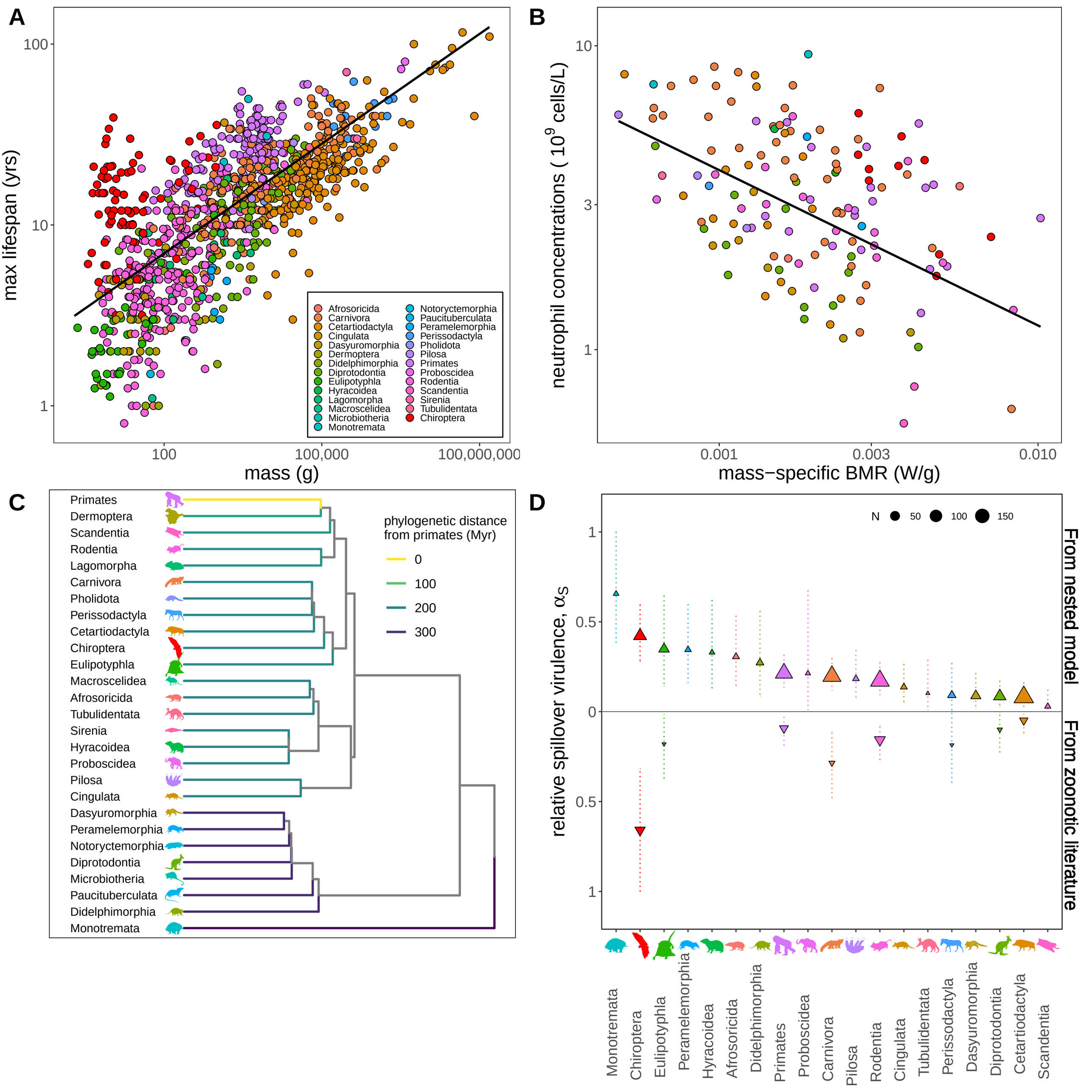
A
max lifespan (yrs)
100
10
1
100
100,000
100,000,000
mass (g)
Afrosoricida
Carnivora
Cetartiodactyla
Cingulata
Dasyuromorphia
Dermoptera
Didelphimorphia
Diprotodontia
Eulipotyphla
Hyracoidea
Lagomorpha
Macroscelidea
Microbiotheria
Monotremata
Notoryctemorphia
Paucituberculata
Peramelemorphia
Perissodactyla
Pholidota
Pilosa
Primates
Proboscidea
Rodentia
Scandentia
Sirenia
Tubulidentata
Chiroptera
B
neutrophil concentrations ( 10^9 cells/L)
10
3
1
0.001
0.003
0.010
mass−specific BMR (W/g)
C
Primates
Dermoptera
Scandentia
Rodentia
Lagomorpha
Carnivora
Pholidota
Perissodactyla
Cetartiodactyla
Chiroptera
Eulipotyphla
Macroscelidea
Afrosoricida
Tubulidentata
Sirenia
Hyracoidea
Proboscidea
Pilosa
Cingulata
Dasyuromorphia
Peramelemorphia
Notoryctemorphia
Diprotodontia
Microbiotheria
Paucituberculata
Didelphimorphia
Monotremata
phylogenetic distance from primates (Myr)
0
100
200
300
D
N
50
100
150
relative spillover virulence, αS
1
0.5
0
0.5
1
From nested model
From zoonotic literature
Monotremata
Chiroptera
Eulipotyphla
Peramelemorphia
Hyracoidea
Afrosoricida
Didelphimorphia
Primates
Proboscidea
Carnivora
Pilosa
Rodentia
Cingulata
Tubulidentata
Perissodactyla
Dasyuromorphia
Diprotodontia
Cetartiodactyla
Scandentia